UC San Diego
UC San Diego Previously Published Works

Title

Folding of the β-Barrel Membrane Protein OmpA into Nanodiscs.

Permalink

Journal

Authors

Asamoto, DeeAnn
Kang, Guipeun
Kim, Judy

Publication Date

DOI

Peer reviewed

Folding of the β-Barrel Membrane Protein OmpA into Nanodiscs

DeeAnn K. Asamoto,[1] Guipeun Kang,[1] and Judy E. Kim[1,*]
[1]Department of Chemistry and Biochemistry, University of California, San Diego, La Jolla, California

ABSTRACT   Nanodiscs (NDs) are an excellent alternative to small unilamellar vesicles (SUVs) for studies of membrane protein structure, but it has not yet been shown that membrane proteins are able to spontaneously fold and insert into a solution of freely diffusing NDs. In this article, we present SDS-PAGE differential mobility studies combined with fluorescence, circular dichroism, and ultraviolet resonance Raman spectroscopy to confirm the spontaneous folding of outer membrane protein A (OmpA) into preformed NDs. Folded OmpA in NDs was incubated with Arg-C protease, resulting in the digestion of OmpA to membrane-protected fragments with an apparent molecular mass of ∼26 kDa (major component) and ∼24 kDa (minor component). The OmpA folding yields were greater than 88% in both NDs and SUVs. An OmpA adsorbed intermediate on NDs could be isolated at low temperature and induced to fold via an increase in temperature, analogous to the temperature-jump experiments on SUVs. The circular dichroism spectra of OmpA in NDs and SUVs were similar and indicated β-barrel secondary structure. Further evidence of OmpA folding into NDs was provided by ultraviolet resonance Raman spectroscopy, which revealed the intense 785 cm^{-1} structural marker for folded OmpA in NDs. The primary difference between folding in NDs and SUVs was the kinetics; the rate of folding was two- to threefold slower in NDs compared to in SUVs, and this decreased rate can tentatively be attributed to the properties of NDs. These data indicate that NDs may be an excellent alternative to SUVs for folding experiments and offer benefits of optical clarity, sample homogeneity, control of ND:protein ratios, and greater stability.

SIGNIFICANCE   Integral membrane proteins constitute a significant fraction of all cellular proteins, yet their folding mechanisms in bilayers remain largely unknown. Studies of the spontaneous in vitro insertion and folding of a model β-barrel membrane protein, OmpA, into lipid bilayers in the absence of molecular chaperones can provide insight into the intrinsic protein-lipid interactions that may help guide the in vivo folding mechanisms. The folding of OmpA into nanodiscs, an improved bilayer mimetic compared to traditional vesicles, opens doors for more extensive studies of membrane protein folding. Enhanced understanding of lipid-protein interactions as well as inter- and intraprotein interactions during folding and insertion events into membrane bilayers would benefit numerous areas of research, such as pathology, medicine, chemistry, biology, and biophysics.

INTRODUCTION

Membrane proteins are integral to key processes of life. They act as regulators of communication between the cell and its environment. Membrane proteins also serve as targets for the majority of pharmaceuticals (1). The biological activity and chemical reactivity of membrane proteins depend on their structure, dynamics, and stability. Improper folding of integral membrane proteins can lead to the development of diseases, such as cystic fibrosis, retinitis pigmentosa, and Charcot-Marie-Tooth disease (2,3).

The characterization of membrane proteins in their native environment is important to better understand their functions and assembly mechanisms. Soluble proteins have been successfully characterized with a variety of experimental methods, such as x-ray crystallography, NMR, and mass spectrometry. However, the insolubility of membrane proteins combined with the complexity of the lipid bilayer makes it difficult to study the dynamics and structures of these biomolecules, including the folding and insertion of membrane proteins in the amphipathic environment of lipid membranes. Another complication is that membrane proteins are not thermodynamically stable in aqueous solution

and easily denature or aggregate outside of the lipid bilayer. These issues are an impediment to comprehensive biophysical studies on membrane proteins; thus, improved methods for study are needed.

Outer membrane protein A (OmpA) is a model protein for studies of membrane protein folding. It is one of the most abundant proteins found in the outer membrane of *Escherichia coli*. OmpA consists of 325 amino acid residues: a transmembrane domain of eight antiparallel β-strands in a barrel and a soluble C-terminal periplasmic domain (4). OmpA is an ideal β-barrel system to study protein folding because it has been previously shown to spontaneously and reversibly fold into synthetic bilayers (5,6) and has been characterized by various biophysical methods. Additionally, wild-type OmpA contains five native tryptophan residues that span the transmembrane domain, and these residues are excellent spectroscopic probes for studies of protein folding.

OmpA spontaneously inserts and folds into small unilamellar vesicles (SUVs), spherical synthetic membrane mimics commonly used to study the in vitro insertion and folding mechanisms of membrane proteins (5–8). It has been proposed that high-curvature membranes are needed for spontaneous folding because of their propensity for defects (5,6,9,10). Preformed SUVs are straightforward to generate in the laboratory, but there are limitations in terms of experimental conditions. They are small (<50 nm diameter) and have high surface curvature, and the turbidity of SUV solutions results in strong Rayleigh scattering that complicates spectral analysis. Additionally, SUVs are thermodynamically unstable, fusing to form larger vesicles, including in the presence of membrane-associated proteins (11,12). OmpA is also able to fold into some large unilamellar vesicles (LUVs) that have a diameter of greater than 100 nm, but the ability to fold into LUVs as well as the kinetics of folding and insertion depend on the hydrocarbon chain (9,10,13). Despite the prevalence of published reports with vesicles, an improved bilayer model could enhance studies of membrane protein folding.

Nanodiscs (NDs) are water-soluble nanoscale discoidal phospholipid bilayers encircled by membrane scaffold proteins or styrene-maleic-acid lipid particles in a belt conformation, first assembled by the Sligar laboratory in 2002 (14). Unlike vesicles, NDs are planar and therefore excellent biological membrane mimics that are well suited for controlled in vitro experiments because of their homogeneity, optical clarity, low light scattering, faster diffusion rates, and greater stability (15,16). NDs have emerged as a valuable membrane mimic, and numerous reports used NDs to incorporate membrane proteins for structural and functional studies. We are aware of a single folding study, published in 2016, that utilized cell-free expression and surface-enhanced infrared absorption spectroscopy to monitor the insertion and folding of bacteriorhodopsin into immobilized NDs on a gold film (17).

In this article, we present sodium dodecyl sulfate polyacrylamide gel electrophoresis (SDS-PAGE) differential mobility studies combined with fluorescence, circular dichroism (CD), and ultraviolet resonance Raman (UVRR) spectroscopy to confirm and characterize the folding reaction of OmpA into NDs. The concerted insertion and folding mechanisms that describe β-barrel membrane protein systems like OmpA have only been discussed using a small set of proteins because of experimental challenges. The study of OmpA in NDs is important because ND technology offers important experimental advantages that enable more extensive studies of membrane protein folding.

MATERIALS AND METHODS

Expression, isolation, and purification of OmpA wild-type and mutants

The expression, isolation, and purification of wild-type and mutant OmpA were performed according to an established procedure (18). The five native tryptophan residues in wild-type OmpA are located at positions 7, 15, 57, 102, and 143. OmpA W129 is a mutant with a single tryptophan residue at a nonnative position (Y129W) and phenylalanine residues at positions 7, 15, 57, 102, and 143 (W7F/W15F/W57F/W102F/W143F). Stock protein solution that contained 130–335 μM protein, 8.0 M urea, and 20 mM potassium phosphate buffer (KP$_i$, pH 7.3) were diluted to appropriate concentrations for our experiments. All reagents were purchased from Thermo Fisher Scientific (Waltham, MA), Genesee Scientific (El Cajon, CA), MP Biomedicals (Santa Ana, CA), and GoldBio (St. Louis, MO) unless otherwise indicated and used without further purification.

Preparation of vesicles and nanodiscs

The procedure for the preparation of SUVs is described elsewhere (18). Briefly, 25 mg of 1,2-dimyristoyl-*sn*-glycero-3-phosphocholine (DMPC) (T$_C$ = 23°C; Avanti Polar Lipids, Alabaster, AL) was dried under nitrogen gas for several hours. A lipid concentration of 5 mg/mL was achieved by resuspending the dried lipid in 5 mL of 20 mM KP$_i$ buffer at pH 8.0. SUVs with ~50 nm diameter were made by sonicating the aqueous lipid solution for 30 min with a probe ultrasonic microtip at 50% duty cycle with 30% maximum amplitude. The vesicles were passed through a 0.22 μm filter and equilibrated at 39°C overnight before use. The identical procedure was followed for 1,2-dipalmitoyl-*sn*-glycero-3-phosphocholine (DPPC) (T$_C$ = 41°C; Avanti Polar Lipids).

LUVs were prepared by resuspending 25 mg of dried DMPC lipid in 20 mM KP$_i$ buffer (pH 8.0) to obtain a 5 mg/mL lipid concentration. The resuspended lipids were bath sonicated for 5 min and extruded through a 0.1 or 0.2 μm pore-size polycarbonate membrane filter (SPI Supplies, West Chester, PA) (19). The lipid solutions were passed through the appropriate membrane filter 22 times using two 5 mL extruder syringes to produce 100- and 200-nm-diameter LUVs. The LUV solutions were equilibrated at 39°C for at least 2 h before use.

Preparation of NDs was based on a published procedure (20). The belt peptide 14A, which is a 14-mer belt peptide with sequence Ac-DYLKAFYDKLKEAF-NH$_2$ (truncated analog of 18A peptide), was purchased from NeoScientific (>98% purity; Cambridge, MA). The appropriate mass of the 14A belt peptide (molecular weight 1792.06 g/mol) was dissolved in 0.7–1.1 mL of 20 mM KP$_i$ at pH 8.0 to create a 10 mg/mL solution. Separately, 25 mg of DMPC (molecular weight 677.95 g/mol) in chloroform was dried under nitrogen gas for several hours to evaporate the solvent. A final DMPC concentration of 6.4 mg/mL was achieved by resuspending the dried lipid

in 3.9 mL of 20 mM KP_i buffer at pH 8.0. An appropriate volume of the 10 mg/mL peptide solution (0.5 mL) was added to 0.5 mL of the 6.4 mg/mL aqueous lipid solution to achieve a final lipid:peptide molar ratio of 1.67 in 1.0 mL of buffer; this lipid:peptide ratio was reported to generate 10-nm-diameter NDs ($T_C = 29°C$ (21)). The NDs were equilibrated at room temperature overnight before use.

Lipid:protein ratios

An important experimental variable in studies of membrane protein folding is the lipid:protein ratio. For these studies, appropriate volumes of stock NDs (4.7 mM lipid) or SUVs (7.4 mM lipid) were added to a buffered solution, followed by the addition of protein to achieve a target lipid:protein ratio. For the majority of the experiments (gel electrophoresis and fluorescence), the target lipid:protein ratio was 300:1 or 400:1; for two experiments, the target ratios were 200:1 (CD), 190:1 (UVRR), or 70:1 (UVRR) because the amount of belt peptide had to be reduced on account of strong CD and UVRR signal from the belt peptide. The actual lipid:protein ratio was determined from a calculated amount of lipid in sample and a measured concentration of protein based on UV-vis absorption spectroscopy (a 1:1 subtraction of the ND or SUV signal from the protein sample isolated the absorbance from OmpA). The 280-nm molar attenuation coefficient for wild-type OmpA is 54,390 cm^{-1} M^{-1} (22). The lipid:protein ratios were within 15% of the target ratios, and two isolated experiments had larger deviations of 30% of the target ratios. For some experiments, such as the digestion studies, the lipid:protein ratios could not be experimentally determined. In this article, the stated lipid:protein ratios are the target ratios. Separate experiments of OmpA folding as a function of lipid:protein ratios were performed to ensure that the 30% variability of actual lipid:protein ratio did not impact the results, as described below.

It is also valuable to consider protein:SUV and protein:ND ratios, which can be determined with assumed input values (see Supporting Materials and Methods for calculations). In all experiments described here, there was less than one OmpA per ND; if a single OmpA were to fold into a ND, the percent coverage of the ND would be 4% for an OmpA pore diameter of 2 nm (based on distance between $C\beta$ atoms across the pore). Depending on the experiment, there was a range of 37–200 OmpA per SUV, with a maximum coverage of 8% of the outer leaflet of the SUV if all 200 OmpA units were to fold into the SUV. The max value of 200 OmpA per SUV was for UVRR experiments that required higher concentration of protein.

Digestion of folded OmpA in SUVs and NDs

Digestion experiments with Arg-C endoproteinase (clostripain) purchased from Protea Biosciences (Morgantown, WV) were performed to confirm that OmpA inserted and folded into NDs. Parallel digestion experiments of OmpA folded into SUVs were performed for comparison. Arg-C was selected as a protease for digestion experiments because it is predicted to specifically cleave at the C-terminal side of arginine residues (23); arginine exists in OmpA but not the ND belt peptide (Fig. 1). Arg-C is described as exhibiting minor activity toward lysine residues (24). Wild-type OmpA was added to preformed ND or SUV solutions in 50 mM ammonium bicarbonate buffer (pH 8.0). For both samples, the lipid:protein ratio and residual urea concentration were 300:1 and 0.3 M, respectively, and the final OmpA concentration was 14 μM. The samples were incubated at 37°C for 6 h, allowing OmpA to fold. The folded state was confirmed with fluorescence and/or SDS-PAGE analysis (see below). After the 6-h folding period, appropriate amounts of these folded stocks were incubated at 37°C with Arg-C to achieve a final OmpA concentration of 9.0 μM (in the presence of NDs) and 8.0 μM (in the presence of SUVs). The final Arg-C concentration was 0.6 μM in the ND sample and 0.5 μM in the SUV sample, which gave OmpA:Arg-C ratios of 15:1 and 16:1, respectively. These OmpA:Arg-C ratios were within the manufacturer-suggested ratio range of 10:1 to 20:1. Digestion of the folded samples in NDs or SUVs with Arg-C was carried out for 3 and 24 h. Dithiothreitol (3.5 μL of
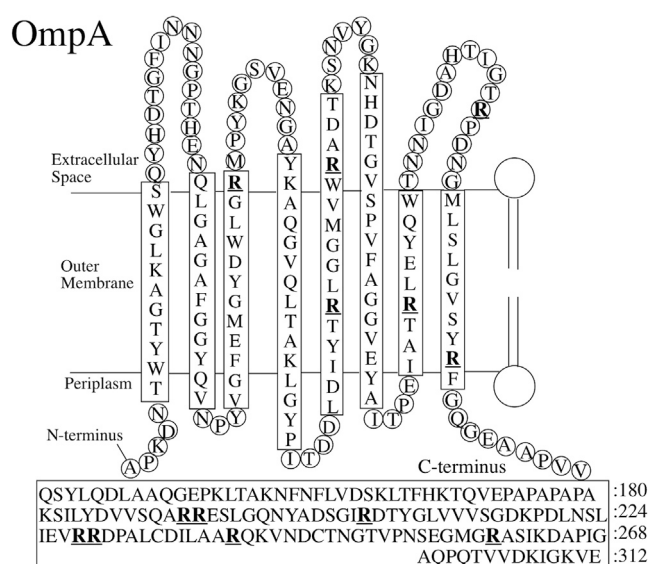
FIGURE 1 The top shows the membrane topology of OmpA. Arginine residues are indicated in bold and are underlined. The bottom shows the primary sequence of 14A, the belt peptide.

1.0 M stock solution) and calcium acetate (4–5 μL of 20 mM stock solution) were added to the samples (final concentrations of 50 and 1.0 mM, respectively) to aid in digestion. A sample of unfolded 5.0 μM OmpA in 3.6 M urea was incubated at room temperature for at least 30 min and digested with Arg-C (OmpA:Arg-C ratio 20:1) at 37°C for 4 h. Approximately 6 μg of the folded protein samples with and without Arg-C was loaded on 12% polyacrylamide Mini-PROTEAN TGX precast gels. For the unfolded samples with and without Arg-C, ∼3.5 μg of protein was loaded on the gel. The samples were not boiled before loading on the gel.

Digestion of adsorbed OmpA on NDs and SUVs

OmpA may be stabilized as an adsorbed intermediate that interacts with but does not insert into a lipid bilayer in the gel phase. Digestion experiments of wild-type OmpA adsorbed onto NDs or SUVs were performed to determine the extent of accessibility of the adsorbed state to Arg-C protease in solution. An aliquot of OmpA from a stock solution was added to equilibrated solutions of NDs or SUVs in ammonium bicarbonate buffer (pH 8.0) at 16°C in a 10 × 4 mm quartz cuvette and sealed with a rubber septum. At 16°C, both DMPC ND and DMPC SUV bilayers are in gel phase, preventing the insertion and folding of OmpA into the bilayer (25). The temperatures of the ND and SUV protein samples were monitored with a thermocouple immersed at the top of the sample (sensor type T with Omega HH201A, Norwalk, CT). Before addition of the protease, the lipid:protein ratio was 300:1, the residual urea concentration was 0.2 M in both ND and SUV samples, and the concentration of OmpA was 8.0 μM. The samples were continuously stirred using a micro stir bar and incubated at 16°C for 4 h before digestion.

Fluorescence spectra of the adsorbed samples were measured after 4 h of incubation, before digestion, at 16°C using a Jobin Yvon-SPEX Fluorolog FL3-11 spectrofluorometer (HORIBA Jobin Yvon Incorporated, Edison, NJ) to confirm the presence of the slightly blue-shifted (relative to unfolded protein) adsorbed intermediate. The samples were excited with a wavelength

of 295 nm along the 4 mm path, and emission was collected along the 10 mm path. The excitation and emission bandpass were set to 3 nm. SDS-PAGE confirmed the absence of folded OmpA via the apparent molecular weight of the adsorbed intermediate, ~33 kDa (5,25), before the addition of Arg-C.

Aliquots of adsorbed OmpA were added to equilibrated solutions of Arg-C protease (OmpA:Arg-C ratio of 10:1) that also contained 50 mM dithiothreitol and 1.5 mM calcium acetate in ammonium bicarbonate buffer (pH 8.0) at 16°C. The final concentrations of OmpA and urea during digestion were 5 μM and 0.1 M, respectively. The samples were incubated at 16°C, and the digested products were analyzed via SDS-PAGE using 12% polyacrylamide Mini-PROTEAN TGX precast gels after 4 and 24 h of digestion. A control sample was analyzed in parallel with the digestion experiment. This control solution was composed of 5 μM OmpA adsorbed onto NDs or SUVs and 0.1 M urea but did not contain Arg-C protease, dithiothreitol, or calcium acetate. Approximately 5 μg of digested and control OmpA was added to the wells. The samples were not boiled before loading onto the gel.

CD spectroscopy

OmpA secondary structure was probed by CD spectroscopy. CD spectra of wild-type and the single-tryptophan mutant, W129, folded in NDs or SUVs and unfolded in 4.0 M urea were obtained with a Jasco J-815 spectrometer (Easton, MD). The sample chamber was continuously purged with nitrogen gas and held at a temperature of 37°C for measurements of folded OmpA. Samples of folded OmpA in NDs or SUVs contained 3–6 μM protein, 0.3 M urea, and 200:1 lipid:protein ratio in 20 mM KP_i buffer (pH 8.0). Samples of unfolded OmpA contained 4–6 μM protein and 4.0 M urea in 20 mM KP_i buffer (pH 8.0). Folded samples were allowed to incubate in the presence of NDs or SUVs at 37°C for 5 h before the collection of CD spectra. Unfolded samples were incubated in their buffered urea solutions for at least 30 min at room temperature before the collection of spectra. CD spectra were acquired from 204 to 260 nm (208–260 nm for unfolded samples) in a 1 mm pathlength quartz cuvette with 1 s digital integration time, 1 nm bandwidth, and 50 nm/min scan speed. A total of six accumulations for each protein sample were collected and averaged. Background samples, which contained the appropriate buffer (including NDs or SUVs for folded samples and urea for unfolded samples) without protein were also acquired and subtracted from each protein spectrum to isolate the signal from protein only. Fluorescence spectra of folded and unfolded protein were also collected to confirm the conformation of each state.

SDS-PAGE differential protein mobility assay during folding

Aliquots of unfolded OmpA from the stock solution were added to buffered (KP_i, pH 8.0), preformed solutions of NDs or SUVs equilibrated at 33°C to achieve an OmpA concentration of 7–15 μM. The lipid:protein ratio in SUVs and NDs was 400:1. This mixing initiated the folding reaction because the urea concentration was diluted to 0.2 M. Samples were maintained at 33°C during the experiment. The folding reaction was quenched at nine time points (t = 4, 8, 16, 30, 46, 60, 120, 180, 240 min after initiation of the folding reaction) by addition of Laemmli loading dye (26) and kept at room temperature until they were loaded onto the gel. The samples were analyzed via SDS-PAGE using 12% polyacrylamide Mini-PROTEAN TGX precast gels at a constant voltage of 150 V with 0.1% SDS in the running buffer. Approximately 3 μg of protein was added to each well of the gel. The gels were stained with Coomassie blue. The samples were not boiled before loading onto the gel.

Fluorescence spectroscopy

The folding reactions of wild-type OmpA in NDs and SUVs were monitored using fluorescence spectroscopy. The folding reactions were initiated by the addition of stock unfolded OmpA into equilibrated ND or SUV solutions. The final samples contained 4 μM OmpA, 0.2 M residual urea, and a lipid:protein ratio of 400:1 in pH 8.0 KP_i buffer. Fluorescence spectra from a Jobin Yvon-SPEX Fluorolog FL3-11 spectrofluorometer were acquired at 10 time points: 1, 4, 8, 16, 30, 46, 60, 120, 180, and 240 min after initiation of the folding reaction. Samples were maintained at 33°C during the 4-h period in a 10 × 2 mm quartz cuvette sealed with a Teflon cap. The samples were excited with 295 nm wavelength light along the 2 mm path, and emission was collected along the 10 mm path. The excitation and emission bandpass were set to 3 nm. Samples were gently shaken before and after fluorescence spectra were acquired to ensure thorough mixing throughout the duration of the experiment. Spectra of NDs and SUVs without OmpA were acquired at the beginning and end of each experiment; these spectra of ND-only and SUV-only were subtracted from OmpA spectra to isolate fluorescence signal from protein. The fluorescence spectrum of folded OmpA in SUVs (98% folding yield based on gel) and unfolded OmpA in 8.0 M urea served as basis spectra for Gaussian decompositions, and all fluorescence data were analyzed by the intensity-corrected decomposition method described elsewhere (27) using Igor Pro software (Wavemetrics, Portland, OR).

Folding reactions of wild-type OmpA in 100- and 200-nm-diameter LUVs were investigated using fluorescence spectroscopy. Appropriate volumes of 5 mg/mL 100- and 200-nm-diameter LUV aqueous solution were added to OmpA stock solutions to yield final OmpA concentrations of 2.0 and 0.5 μM, respectively. The lipid:protein ratios were 1250:1 (100-nm LUV) and 5000:1 (200-nm LUV); these ratios were selected to maintain the same vesicle:OmpA ratio of 1:49 for all three vesicles, including SUVs. A sample of 5 μM OmpA with SUVs (lipid:protein ratio of 300:1) was also prepared for comparison. The residual urea concentration in all samples was 0.2 M. The OmpA-LUV and OmpA-SUV samples were incubated overnight for 12 h at 33°C in a temperature-controlled water bath. After the 12-h folding period, fluorescence spectra were measured for each sample. All samples were excited with 290 nm light along the 2 mm pathlength and emission was collected from 305 to 500 nm along the 10 mm pathlength. The excitation and emission bandpass were set to 3.5 nm. Spectra of vesicles only in 0.2 M urea and 20 mM KP_i (pH 8.0) were also acquired, and these spectra were used to remove background scattering and isolate signal from protein-only.

Fluorescence spectra of wild-type OmpA were acquired above and below the transition temperature for the lipid bilayers. The temperature of the samples was monitored with a thermocouple inserted at the top of the sample. Stock unfolded wild-type OmpA was added to an equilibrated solution of NDs or SUVs (pH 8.0) at 15°C in a 10 × 4 mm quartz cuvette and sealed with a rubber septum. After mixing, the samples contained 4 μM OmpA and 0.2 M urea. The lipid:protein ratio in both ND and SUV samples was 300:1. The samples were excited with 295 nm light along the 4 mm path, and emission was collected along the 10 mm path. The excitation and emission bandpass were set to 3 nm. Fluorescence spectra were acquired at 15°C at times 2, 3, and 4 h after addition of protein. The temperature was then raised to 36°C, and fluorescence spectra were acquired after 2 and 4 h at this elevated temperature. Samples were gently shaken before and after spectra were acquired to ensure thorough mixing throughout the experiment. Spectra of ND-only and SUV-only in 0.2 M urea were also acquired at the same time points and temperatures as protein solutions. The ND-only and SUV-only spectra were used for background subtraction.

UVRR spectroscopy

UVRR spectroscopy was employed to further confirm the folding of OmpA into NDs. The UVRR Ti:sapphire laser system has been previously described (28). A 228-nm excitation beam was used to measure the UVRR spectra of OmpA mutant W129. This mutant was selected for UVRR experiments because it exhibits an intense and unique peak at 785 cm^{-1} that is indicative of folded protein (7). Protein samples of 20 μM W129 OmpA were prepared in four aqueous solutions that contained 10 mg/mL N-octyl-β-D-glucoside

(OG) detergent micelles with 0.8 M urea, 1 mg/mL DMPC SUVs (lipid:protein ratio of 70:1) with 0.8 M urea, 1 mg/mL DPPC SUVs (lipid:protein ratio of 70:1) with 0.8 M urea, and 0.8 M urea. Experiments with DPPC probed the adsorbed state of OmpA on SUVs. The 1.3 mg/mL DMPC ND samples contained 10 μM OmpA with 0.6–0.8 M urea and a lipid:protein ratio of 190:1. All UVRR spectra were collected for 10 min, with the exception of the OmpA in ND samples, which were collected for 5 min.

RESULTS

Digestion of folded OmpA

The extent of protection of the OmpA transmembrane domain in NDs and SUVs was investigated with digestion experiments. Arg-C protease selectively cleaves at arginine sites and is reported to also cleave at lysine sites at slower rates (29). Fig. 1 shows that there are 13 arginine residues in OmpA, with five arginine residues predicted to be in the transmembrane domain and thus protected from digestion in the folded state. SDS-PAGE bands that correspond to OmpA folded in NDs, folded in SUVs, folded and digested, unfolded in 3.6 M urea, and unfolded and digested are shown in Fig. 2. The differential mobility shift of folded (~29 kDa) and unfolded (~33–35 kDa in the presence of 3.6 M urea) OmpA (calculated MW of 35,172 Da) is consistent with previous studies (5,25,30), and is attributed to the increase in compactness in the native form relative to the denatured conformation (31). Analysis of the optical band densities in Fig. 2 using UN-SCAN-IT gel analysis software determined the folding yield to be 89% in NDs and 96% in SUVs. Folded OmpA in NDs or SUVs incubated with Arg-C for 3 or 24 h was digested to a protected major ~26 kDa fragment and a minor ~24 kDa fragment; the native ~29 kDa folded band was eliminated with Arg-C digestion. The first exposed arginine residue outside the membrane-protected region of OmpA is position 242, and the resulting folded fragment has a calculated MW of 26,300 Da. Given that folded OmpA exhibits an apparent MW that is typically lower than the calculated MW on gels, the observed values of ~26 and ~24 kDa bands correspond to membrane-protected fragments. A 24 kDa membrane-protected portion of OmpA has been previously published with trypsin as the cleaving enzyme (5,25). The observation of a smaller membrane-protected fragment with trypsin (24 kDa) compared to Arg-C (~26 kDa) is consistent with the presence of several lysine residues (positions 192, 197, 206, 210, 230) that precede the first exposed arginine residue (position 242), resulting in a smaller membrane-protected fragment with trypsin. Unfolded OmpA in the presence of Arg-C was digested to fragments with apparent molecular weights of 10–17 kDa (data not shown).

Digestion of OmpA adsorbed intermediate

Digestion experiments were carried out to determine the accessibility of Arg-C protease to adsorbed OmpA. Gels in
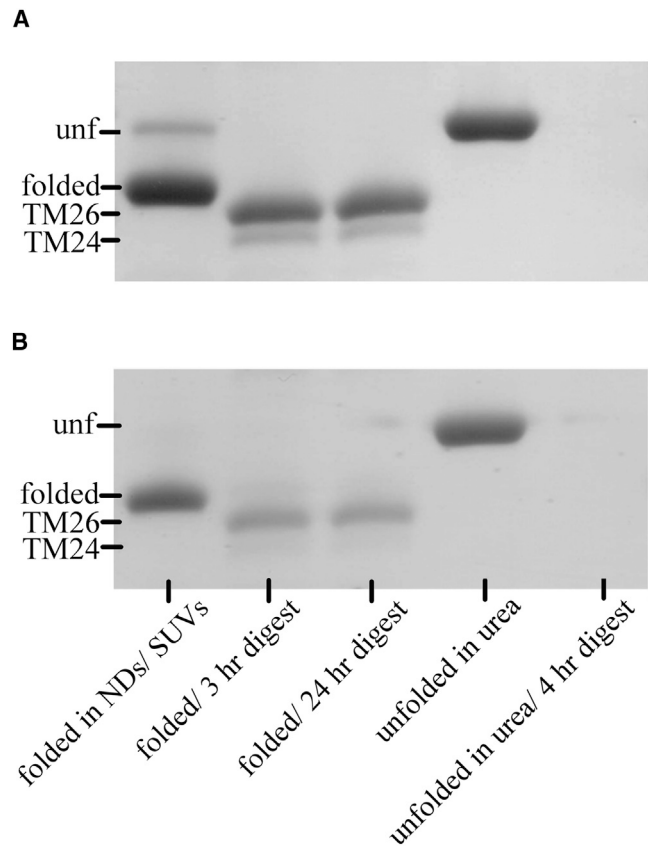

FIGURE 2 SDS-PAGE result of OmpA digestion. Gels show digestion of OmpA in NDs (A) and in SUVs (B). The lipid:protein ratio was 300:1 and the residual urea concentration was 0.3 M before digestion. Samples during folding and digestion were incubated at 37°C. For both gels: lane 1: folded in NDs (A) or in SUVs (B); lane 2: folded in NDs (A) or SUVs (B) and digested with Arg-C for 3 h; lane 3: folded in NDs (A) or SUVs (B) and digested with Arg-C for 24 h; lane 4: unfolded (unf) OmpA in 3.6 M urea; and lane 5: unf OmpA in 3.6 M urea and digested with Arg-C for 4 h. The bands for folded, unf, and the ~26- and ~24-kDa transmembrane fragments (TM26 and TM24) are indicated.

Fig. 3 show bands near 35 kDa, which correspond to OmpA adsorbed (5) onto DMPC SUVs and NDs. After 4 h of digestion with Arg-C protease at 16°C, the intensities of the bands for adsorbed OmpA are significantly decreased. After 24 h of digestion at 16°C, the adsorbed band is completely eliminated.

Folding of OmpA in NDs and SUVs

The secondary structure of wild-type OmpA in NDs and SUVs was investigated with CD. The CD spectra for folded OmpA exhibited a minimum near 215 nm, characteristic of folded OmpA (Fig. S1; (22,32)). The CD spectrum of OmpA unfolded in the presence of urea exhibited a large negative feature that extends into the far UV region, and this feature has been attributed to denatured OmpA (22,32).

The insertion and folding of wild-type OmpA into NDs and SUVs was monitored at 33°C for 4 h by SDS-PAGE differential mobility studies. A representative data set is shown

Adsorbed on NDs
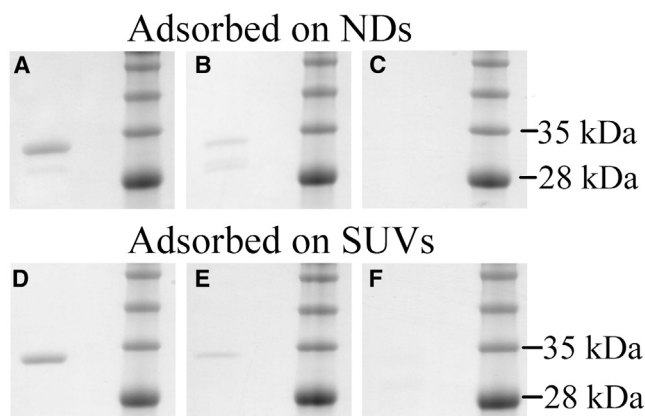
Adsorbed on SUVs

FIGURE 3 Arg-C digestion of wild-type OmpA adsorbed on NDs (*top*) and SUVs (*bottom*) at 16°C. In each image, the left lane contains protein, and the right lane is the molecular weight ladder. Gels are of OmpA adsorbed on (*A*) NDs, no digestion; (*B*) NDs, 4-h digestion; (*C*) NDs, 24-h digestion; (*D*) SUVs, no digestion; (*E*) SUVs, 4-h digestion; and (*F*) SUVs, 24-h digestion. The residual urea concentration in the samples before digestion was 0.2 M.

in Fig. 4. The folding reaction was initiated by mixing protein with equilibrated ND or SUV samples; this mixing resulted in a reduction in urea concentration to 0.2 M. The conversion of denatured to native conformation is evident in protein bands at the two distinct apparent molecular weights of ~33 and ~29 kDa, respectively, based on calculated R_f values. The fraction of folded OmpA at different time points during the folding reaction was assessed by density analysis of the bands, and the evolution of population was fit to a single exponential function. The folding time, τ, is the reciprocal rate constant ($1/k$) and was 28 ± 4 min (five trials); the folding yield was $88 \pm 12\%$ (seven trials) for OmpA in NDs. Analogous values for OmpA in SUVs were 10 ± 5 min (three trials) for the folding rate and $97 \pm 2\%$ (four trials) for the folding yield. These results are summarized in Table 1.

The folding reaction of OmpA was also investigated with fluorescence spectroscopy. The folding of OmpA into SUVs and LUVs has been previously reported (9,10,22,30,33,34), and it is well known that there is a characteristic emission λ_{max} blue-shift and increase in fluorescence quantum yield upon folding (27). Fig. 5 shows representative fluorescence spectra of OmpA in the presence of NDs and SUVs and illustrates the λ_{max} blue-shift from 356 nm (in 8 M urea) to 337 nm (in SUVs and NDs) over 4 h. These experimental fluorescence spectra were decomposed into two Gaussian, intensity-weighted basis spectra for fully folded (337 nm) and unfolded (357 nm) spectra, where the fully folded spectrum exhibited an increased fluorescence quantum yield by a factor of 3.2 relative to unfolded OmpA. This decomposition method has been used to determine the fraction of folded protein during folding (27). The folding rate ($\tau = 1/k$) based on single exponential fit was 21 ± 5 min (four trials), and the folding yield was $97 \pm 2\%$ (four trials) for OmpA in
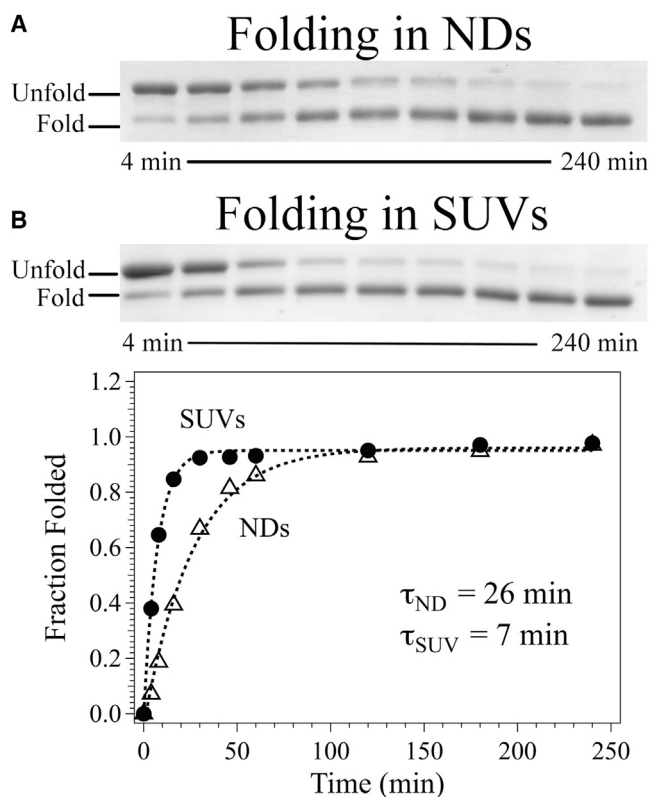
FIGURE 4 Wild-type OmpA folding reaction monitored by SDS-PAGE at 33°C for 4 h. Data were collected at 4, 8, 16, 30, 46, 60, 120, 180, and 240 min after initiation of the folding reaction. The top shows SDS-PAGE gels of OmpA folding in the presence of (*A*) NDs and (*B*) SUVs. The bottom shows fraction folded based on gel band densities for OmpA in NDs (*triangles*) and SUVs (*solid circles*). The lipid:protein ratio in SUVs and NDs was 400:1 and the residual urea concentration was 0.2 M. The curves and resulting folding times are based on single exponential fits to the data, including a value of 0 at time 0 min.

NDs. Analogous values for folding rate and yield for OmpA in SUVs were 9 ± 4 min (three trials) and $99 \pm 1\%$ (three trials), respectively. Representative decompositions of OmpA in NDs are shown in Fig. S2. Use of alternate functions, such as the log-normal function as opposed to Gaussian, did not affect the resulting kinetics. The kinetic parameters are summarized in Table 1.

The dependence of folding rates and yields on different lipid:protein ratios were also investigated with SDS-PAGE differential mobility and fluorescence measurements. Actual lipid:protein ratios of 70:1, 170:1, 230:1, and 300:1 were confirmed by absorption spectroscopy, and results of folding experiments are shown in Fig. S3. The yields of folding after 4 h of incubation was 94–97% based on gels and 98–100% based on fluorescence; these are high folding yields regardless of lipid:protein ratio. The folding rate assessed by fluorescence did depend on the lipid:protein ratio when the ratio was low; at the lowest ratio of 70:1, the folding rate was 36 min, whereas for the higher ratios of 170:1, 230:1, and 300:1, the rates were similar at 26, 22, and 20 min, respectively.
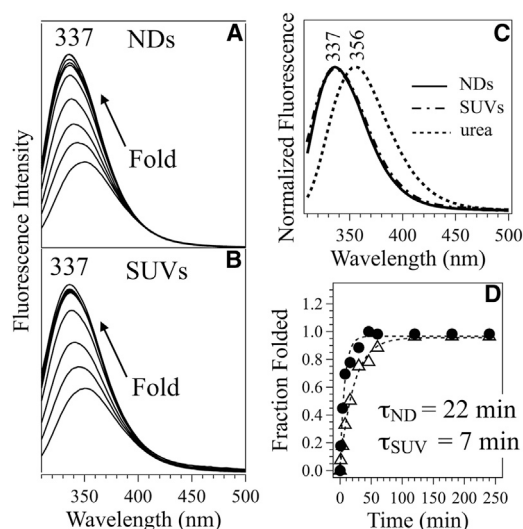
TABLE 1 Summary of Folding Time Constants and Yields for Wild-Type OmpA in DMPC Bilayers

	NDs	SUVs
SDS-PAGE		
τ (min)	28 ± 4 ($n = 5$)	10 ± 5 ($n = 3$)
Folding yield (%)	88 ± 12 ($n = 7$)	97 ± 2 ($n = 4$)
Fluorescence		
τ (min)	21 ± 5 ($n = 4$)	9 ± 4 ($n = 3$)
Folding yield (%)	97 ± 2 ($n = 4$)	99 ± 1 ($n = 3$)

The results were determined by SDS-PAGE differential mobility studies and fluorescence spectroscopy. The data from SDS-PAGE gels were quantified using UN-SCAN-IT gel analysis software. The data from fluorescence spectra were quantified via Gaussian decompositions. τ is the reciprocal rate constant, $1/k$, based on the exponential fit and is reported as $\tau \pm$ standard deviation for the indicated number of n trials; a value of 0 was included at time 0 min in the fits. The reported folding yields are the average of the fraction folded at 240 min for each of the trials.

The folding of OmpA into lower curvature, 100-nm- and 200-nm-diameter LUVs, was probed with fluorescence spectroscopy. Fig. S4 shows that the emission maxima of OmpA in LUVs are 342 and 341 nm. These wavelengths are red shifted relative to the λ_{max} value of 337 nm in the presence of SUVs.

The ability to initiate folding of adsorbed OmpA by converting the bilayer to the fluid phase was investigated with variable-temperature fluorescence experiments. Previous fluorescence reports demonstrated that the low-temperature intermediate form of OmpA can be converted to native, folded OmpA by increasing the temperature above

the phase transition of the bilayer (35). Fig. S5 shows fluorescence spectra corresponding to the low-temperature adsorbed intermediate on NDs and SUVs. The adsorbed intermediate is characterized by fluorescence λ_{max} values of 343 (NDs) and 345 (SUVs) nm. The adsorbed species was formed rapidly (35) and over the course of 4 h at 15°C, the fluorescence λ_{max} emission and quantum yield did not change significantly. When the ND and SUV sample temperatures were increased above the phase transition of the bilayer to 36°C, the fluorescence λ_{max} emission values shifted to 337 nm and the quantum yield increased.

UVRR spectroscopy of folded OmpA

The folding of OmpA into NDs was further investigated with UVRR spectroscopy. Single-tryptophan mutant W129 was selected for this analysis because this mutant exhibits a unique peak at 785 cm^{-1} that is assigned a hydrogen-out-of-plane (HOOP) mode (18,36) for natively folded protein. The mutant W129 exhibited similar folding kinetics, yield, and secondary structure as wild-type (Figs. S1 and S6). Fig. 6 shows UVRR difference spectra of W129 in various conformations of folded, adsorbed, and unfolded. The HOOP mode is observed only under folding conditions in the presence of OG detergent micelles, DMPC SUVs, and DMPC NDs. Other prominent UVRR bands, labeled W18, W17, and W7, are indicated. Additional UVRR spectra for a tryptophan + tyrosine mixture to mimic OmpA mutant W129, 10 mg/mL OG detergent, 1 mg/mL DMPC SUVs, and 20 mM KP$_i$ buffer can be found in Fig. S7.

DISCUSSION

The results from this study indicate that OmpA spontaneously inserts and folds into NDs with similar yield and ~2- to 3-fold decreased rate as into SUVs. This finding is significant because the majority of research on NDs and membrane proteins typically focuses on structure and function of membrane proteins (37–39) and not on the process of folding. Our data indicate that NDs can also elucidate dynamics of protein folding and are an excellent alternative to vesicles with additional benefits of homogeneity, optical clarity, better control of ND:protein ratio, and greater stability.

OmpA folding into bilayers

Several factors influence the yield and kinetics of the folding of OmpA into lipid bilayers, including pH, temperature, lipid headgroup, lipid chain length, lipid concentration, and lipid saturation (9,32,40). The impact of membrane thickness and vesicle curvature on the rates of formation of OmpA secondary and tertiary structures has been investigated (9). Fluorescence, CD, and gel electrophoresis showed that OmpA does not spontaneously insert and fold into low-

FIGURE 5 Wild-type OmpA folding reaction monitored by fluorescence spectroscopy at 33°C for 4 h. Spectra were acquired 1, 4, 8, 16, 30, 46, 60, 120, 180, and 240 min after initiation of the folding reaction in DMPC NDs (*A*) or SUVs (*B*). The lipid:protein ratio was 400:1 and the residual urea concentration was 0.2 M for both samples. The steady-state spectra of OmpA folded in NDs and SUVs and unfolded in 8 M urea are shown in (*C*). The fraction folded during folding reactions in SUVs (*solid circles*) and NDs (*triangles*) are shown in (*D*), with single exponential fits (including a value of 0 at time 0 min).
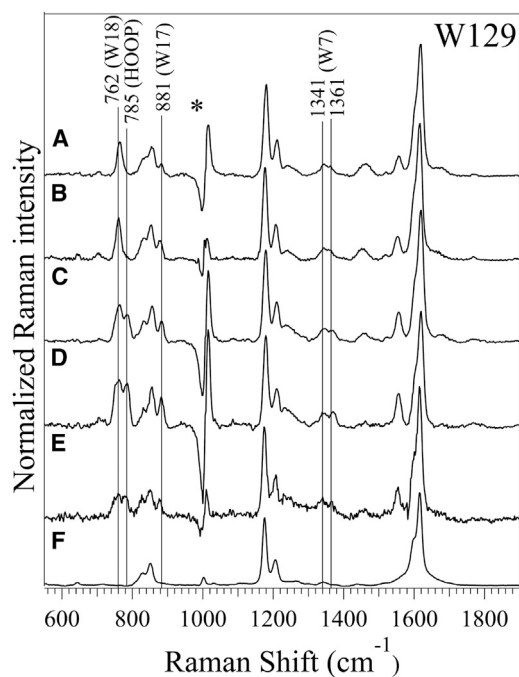
FIGURE 6 UVRR difference spectra. Signal from the buffer, urea, SUVs, and NDs as well as general scattering have been subtracted for OmpA W129 mutant in (*A*) 0.8 M urea, (*B*) adsorbed on DPPC SUVs, (*C*) folded in detergent (OG), (*D*) folded in DMPC SUVs, and (*E*) folded in DMPC NDs. The spectrum of ND-only in which signal from buffer is subtracted is shown as (*F*). All spectra were collected at room temperature and for 10 min, with the exception of the spectrum of OmpA in NDs (*E*), which was collected for 5 min. The region near 1000 cm^{-1} (indicated with *) has strong urea signal in each sample except (*F*), resulting in a subtraction artifact.

curvature LUVs that contain lipid chains with more than 12 carbon atoms, such as DMPC. However, when these long-chain lipids of >12 carbons were incorporated into high-curvature SUVs, OmpA successfully folded into these SUVs (9). Additional studies showed that high curvature is not required for folding; when LUVs were composed of short-chain lipids of 12 or fewer carbon atoms, OmpA was able to insert and fold into these LUVs (9,10). The enhanced folding rates and yields in thin or highly curved bilayers are attributed to bilayer defects; the transient pores and flexibility that result from the defects facilitate folding (6,9,34,41).

Properties of NDs

Discoidal planar NDs formed from the membrane scaffold protein 18A, which is an α-helical peptide derived from apolipoprotein A-1, have been previously described (42,43). It was shown by NMR and single-particle electron microscopy that the 14-residue amphipathic truncated analog of 18A, referred to as 14A, (Fig. 1 *B*) is able to generate stable 10-nm-diameter planar NDs when mixed with DMPC lipids at a lipid:peptide molar ratio of 1.67 (20,44). Based on the circumference of the 10-nm-diameter

ND and using typical properties of an α-helix (e.g., 3.6 amino acids per turn, pitch of 5.4 Å), the scaffold belt may consist of up to 28 α-helical 14A peptides (14 peptides per single belt and 2 belts per ND). The ND double belt arrangement of 14A using DMPC lipid was confirmed by solid-state NMR spectroscopy (45). To the best of our knowledge, extensive biophysical studies of the 14A peptide in NDs have not been published, certainly not to the extent as the 18A peptide. Hence, we rely on findings of 18A to help understand the properties of the 14A peptide.

The properties of NDs composed of the 18A belt peptide have been compared to those of vesicles. Förster resonance energy transfer experiments on NDs with the 18A belt peptide and 1-palmitoyl-2-oleoyl-*sn*-glycero-3-phosphocholine (POPC) showed that NDs have a higher lipid-exchange rate by a factor of 20 compared to vesicles; the rate of exchange in NDs is ~20 min compared to 440 min for vesicles (44). The collision-induced, enhanced lipid exchange between NDs was ascribed to the discontinuities between the multiple belt peptides that constitute the overall ND belt (44). The membrane surface packing state and hydration level of NDs consisting of 18A peptide were probed by fluorescence lifetime experiments, and the results indicated that these NDs were more similar to planar NDs and LUVs as opposed to curved or the "saddle" surface of NDs that are generated with longer belt peptides (44).

The fluidity of NDs differs from liposomes, and this variation has been attributed to the presence of the scaffold peptide belt that can impact the motions of the lipid chains enveloped by the belt. Solid-state NMR experiments have shown that NDs exhibit greater lipid internal ordering than liposomes at 298 K (above the lipid phase transition) (46). The same study showed that both fluid and gel-phase bilayer characteristics exist at temperatures below the phase transition of an ND using the scaffold protein MSP1ΔH5. These results are consistent with the general finding that NDs exhibit broader and higher phase transition temperatures compared to large vesicles on account of the presence of the scaffold belt and loss of cooperativity of the lipids of NDs because of their small size (21,37,46).

OmpA folds into NDs and SUVs

The spectroscopic and gel data presented here indicate that OmpA successfully folds into NDs. Fluorescence spectra reveal changes in environment for tryptophan residues in OmpA in the presence of NDs. As tryptophan inserts into a hydrophobic lipid environment from polar water, there is an observed fluorescence blue-shift from ~350 nm in water to ~330 nm in the lipid bilayer with a typical increase in fluorescence quantum yield (27). The background-corrected fluorescence spectra during the folding reaction of OmpA into NDs and SUVs are shown in Fig. 5. The earliest time point taken at 1 min after initiation of the folding reaction into NDs and SUVs exhibits λ_{max} values of 351 and

352 nm, respectively. These emission maxima are higher in energy than OmpA unfolded in urea, where λ_{max} is 356 nm. This fast initial blue-shift of λ_{max} relative to OmpA in urea is indicative of OmpA interaction with the lipid bilayer before the insertion and folding process (7). The fluorescence data presented here agree with previous characterization of an OmpA membrane-bound intermediate adsorbed to a DOPC lipid bilayer surface within 1 or 2 min after initiation of the folding reaction (47). After ~1 h in the presence of NDs or SUVs, the values for λ_{max} are the most blue-shifted at 337 nm. This 19 nm emission blue-shift relative to OmpA in urea is consistent with literature values reported for OmpA folded in the bilayer (7,18,22,27). The initial binding of OmpA to a membrane surface (within minutes) and the sequential slow step of folding (within hours) agree with published results (8,35,47,48). Based on the intensity-weighted decomposition method (27) of the tryptophan fluorescence, nearly identical folding yields of 97 $\pm$ 2% (NDs) and 99 $\pm$ 1% (SUVs) were observed. The folding rate into NDs was slower, with an exponential rise time of 21 $\pm$ 5 min, compared to SUVs, which had an exponential rise time of 9 $\pm$ 4 min.

The results from fluorescence, which reveal changes in local environment for tryptophan residues, can be compared to results from SDS-PAGE differential mobility studies, which measure global structure. The observation of native (in SUVs) and unfolded (in urea) OmpA as two distinct bands on a gel has been previously documented (5,6,25). The calculated folding yield of OmpA based on gel band densities are 88 $\pm$ 12% (NDs) and 97 $\pm$ 2% (SUVs). The average yield for folding into NDs as assessed by gel band density is 9% lower than the average yield based on fluorescence (97 $\pm$ 2%), but within one standard deviation given the large spread of yields in NDs. The folding rates are also noticeably slower for NDs compared to SUVs.

The kinetics probed by fluorescence reveal changes in local environment of tryptophan, whereas the kinetics obtained by gel mobility experiments reflect changes in the formation of global structure. The faster folding rate in NDs reported by fluorescence reflects the expectation that adsorption and partial insertion of OmpA into the bilayer precedes the formation of OmpA global structure (49). The observation that the folding yields are greater than 88% for the two independent methods of gels and fluorescence gives confidence that OmpA folds successfully into NDs.

Native OmpA in NDs

Three independent experiments indicate that OmpA is folded with the same structure in NDs as in SUVs. One experiment is UVRR, which reveals the vibrational structure of biomolecules; excitation with 228 nm selectively enhances Raman signal from aromatic residues, in particular tryptophan, with minimal contribution from protein back-bone and buffer. UVRR complements fluorescence spectroscopy (local environment) and gel mobility studies (global structure) by revealing site-specific information and noncovalent molecular interactions.

The single-tryptophan mutant, W129, was studied by UVRR because this nonnative tryptophan residue exhibits a unique peak present at 785 cm^{-1}, near the shoulder of the W18 mode, which we have interpreted as an enhanced HOOP mode. This HOOP mode is only present for tryptophan residues at positions 129 and 15 and only when OmpA is folded (Fig. 6; (18,36,50)). When OmpA is unfolded in urea or adsorbed onto DPPC SUVs, the vibrational peak at 785 cm^{-1} is absent. Thus, this HOOP mode can be utilized as a marker to indicate whether OmpA folded into NDs. The W129 HOOP mode appears only under folding conditions in the presence of micelles, SUVs, and NDs. We hypothesize that this HOOP mode gains intensity because of the perturbation of the indole π electrons resulting from an interaction with a nearby charge during folding (51). This perturbation is most likely induced by intramolecular interactions rather than intermolecular interactions, such as protein-lipid interactions, because the mode is intense when OmpA is folded in OG micelles, and OG has no charged groups. The mode is also intense when OmpA is folded in DMPC SUVs, which have zwitterionic headgroups. One possible explanation for the enhanced HOOP intensity is that a charged residue of the protein in the vicinity of the nonnative tryptophan placed at position 129 interacts with the indole side chain and perturbs the vibrations.

Structural insights were also gained through digestion studies and CD measurements. In the presence of Arg-C, a membrane-protected fragment remained in both NDs and SUVs. This observation indicates that OmpA has the same general inserted structure in both environments. The β-barrel secondary structure is preserved in NDs, as shown in CD spectra (Fig. S1). The CD spectra also highlight an important benefit of NDs; the highly scattering nature of SUVs is a known challenge to CD spectra (52,53), and this challenge is overcome by using optically clear ND samples. The poor S/N of the CD spectra in SUVs at 205–210 nm can be contrasted with the smooth curve for NDs in the same wavelength range.

The finding that OmpA retains similar structure in NDs as in SUVs complements the general conclusions from NMR studies that have confirmed similar OmpA structure in NDs and detergent micelles and bicelles. Sequence-specific NMR assignments provided evidence of near-identical polypeptide backbone conformations for OmpA and OmpX in NDs and detergent micelles (54). A second NMR structural study confirmed that the two independently folded N- and C-terminal domains of OmpA were connected via a flexible linker, with the C-terminus periplasmic domain correctly located outside the membrane in both micelles and NDs (55).

Folding of the OmpA adsorbed intermediate

The adsorbed intermediate refers to OmpA that interacts with the surface of the bilayer but is not inserted into the hydrocarbon core; this species is generated when the bilayer is in the gel phase, below the phase transition temperature to the fluid phase. The adsorbed intermediate has been shown to consist of β-sheet secondary structure and is completely degradable by trypsin (40) and Arg-C protease in solution (as shown in Fig. 3). The OmpA adsorbed intermediate in the presence of DPPC SUVs exhibits a fluorescence emission that is blue-shifted by up to 13 nm relative to unfolded OmpA in urea and exhibits similar secondary structure to the folded protein (5,7). Similarly, the fluorescence emission of OmpA adsorbed onto DMPC LUVs after 12 h of incubation in the presence of 100- and 200-nm-diameter LUVs is 342 and 341 nm, respectively (blue-shift of ~14 nm relative to unfolded OmpA in urea; Fig. S4). The fluorescence maxima of the OmpA adsorbed intermediate on gel-phase DMPC SUVs and DMPC NDs are blue-shifted 11 and 13 nm, respectively, relative to unfolded OmpA in urea. These values are consistent with previously reported values of an OmpA adsorbed intermediate (25). The adsorbed intermediate that is trapped at low temperature on gel-phase DMPC SUVs can be initiated to fold via an increase in temperature to the fluid phase (35). We have performed analogous experiments for NDs, and the data indicate that the folding behavior is similar to SUVs; the adsorbed intermediate on NDs can also be isolated at low temperatures ($<T_C$) and converted into native OmpA by raising the temperature above T_C (Fig. S5). These data indicate that the OmpA adsorbed intermediate may be valuable as an initial state for folding experiments.

Comparison of NDs and SUVs

The data presented here indicate that the folding reaction of OmpA into NDs exhibits no noticeable differences compared to SUVs in terms of 1) folding yield as measured by fluorescence; 2) folding yield as assed by gels; 3) secondary and tertiary structures as assessed by CD, gels, and UVRR; and 4) the adsorbed intermediate as assessed by low-temperature fluorescence experiments and gels. The only difference was the folding rates assessed by gels and fluorescence, for which folding in NDs was ~2- to 3-fold slower (28 $\pm$ 4 min for gels and 21 $\pm$ 5 min for fluorescence) compared to in SUVs (10 $\pm$ 5 min for gels and 9 $\pm$ 4 min for fluorescence). The conclusion that OmpA successfully folds into DMPC NDs is somewhat surprising given that OmpA does not fold into DMPC LUVs (9,10); both LUV and ND bilayers are considered flat, with decreased exposure of hydrophobic chains relative to high-curvature SUVs (9), and with equivalent hydration levels (44). However, one important difference between LUVs and NDs is that lipids in NDs are more dynamic

compared to LUVs as revealed by the 20-fold greater lipid-exchange rate in NDs (44). Although the belt peptide results in more packed and ordered lipids (46), the discontinuities at the edge of the ND may give rise to the defects near the edges that not only enhance lipid exchange but also facilitate the folding of OmpA. The observation of the two- to threefold decrease in folding rate in NDs compared to SUVs indicates there may be a larger barrier to fold into NDs. However, the high yield of folding into NDs and SUVs combined with the spectroscopically undifferentiable structures in both types of bilayers suggests that the thermodynamically favored conformation of OmpA is equivalent in NDs and SUVs.

The ability to perform folding experiments in NDs offers experimental advantages. With less than one OmpA per ND, there is no crowding or other protein-protein effects on the folding reaction, thus simplifying the interpretation of data. Additionally, the size of the ND can be varied by adjusting the ratio of the lipid:scaffold peptide or by altering the length of the scaffold peptide to incorporate different sizes of membrane proteins (20,38,39). The inherently homogenous and stable NDs enable reproducible and extended experiments that are sometimes challenging to accomplish with thermodynamically unstable SUVs. The optical clarity of NDs is another important benefit because optical experiments, such as absorption, CD, and vibrational spectroscopy, can be pursued with minimal artifacts. These and other improvements in experimental conditions for membrane protein folding will help unveil new insights into this fundamental process in biology.

Summary

The findings presented here indicate that OmpA spontaneously inserts and folds into NDs with comparable yield and a two- to threefold slower rate relative to SUVs. The results from SDS-PAGE mobility, digestion, steady-state fluorescence, UVRR, and CD studies suggest the OmpA secondary and tertiary structures are preserved upon folding in NDs. These data indicate that NDs may be an improved alternative to commonly used SUVs for studies of membrane protein folding because of the inherent stability and homogeneity of NDs.

SUPPORTING MATERIAL

AUTHOR CONTRIBUTIONS

D.K.A. performed all experiments and analyzed the corresponding data. G.K. contributed to the initial experiments in this project and collected and analyzed the UVRR data for OmpA in detergent, SUVs, and urea. J.E.K. is the corresponding author and guided all experiments.

ACKNOWLEDGMENTS

REFERENCES

1. Arinaminpathy, Y., E. Khurana, …, M. B. Gerstein. 2009. Computational analysis of membrane proteins: the largest class of drug targets. *Drug Discov. Today.* 14:1130–1135.

2. Marinko, J. T., H. Huang, …, C. R. Sanders. 2019. Folding and misfolding of human membrane proteins in health and disease: from single molecules to cellular proteostasis. *Chem. Rev.* 119:5537–5606.

3. Schlebach, J. P., D. Peng, …, C. R. Sanders. 2013. Reversible folding of human peripheral myelin protein 22, a tetraspan membrane protein. *Biochemistry.* 52:3229–3241.

4. Koebnik, R., K. P. Locher, and P. Van Gelder. 2000. Structure and function of bacterial outer membrane proteins: barrels in a nutshell. *Mol. Microbiol.* 37:239–253.

5. Surrey, T., and F. Jähnig. 1992. Refolding and oriented insertion of a membrane protein into a lipid bilayer. *Proc. Natl. Acad. Sci. USA.* 89:7457–7461.

6. Surrey, T., and F. Jähnig. 1995. Kinetics of folding and membrane insertion of a beta-barrel membrane protein. *J. Biol. Chem.* 270:28199–28203.

7. Sanchez, K. M., G. Kang, …, J. E. Kim. 2011. Tryptophan-lipid interactions in membrane protein folding probed by ultraviolet resonance Raman and fluorescence spectroscopy. *Biophys. J.* 100:2121–2130.

8. Dewald, A. H., J. C. Hodges, and L. Columbus. 2011. Physical determinants of β-barrel membrane protein folding in lipid vesicles. *Biophys. J.* 100:2131–2140.

9. Kleinschmidt, J. H., and L. K. Tamm. 2002. Secondary and tertiary structure formation of the beta-barrel membrane protein OmpA is synchronized and depends on membrane thickness. *J. Mol. Biol.* 324:319–330.

10. Pocanschi, C. L., G. J. Patel, …, J. H. Kleinschmidt. 2006. Curvature elasticity and refolding of OmpA in large unilamellar vesicles. *Biophys. J.* 91:L75–L77.

11. Lentz, B. R., T. J. Carpenter, and D. R. Alford. 1987. Spontaneous fusion of phosphatidylcholine small unilamellar vesicles in the fluid phase. *Biochemistry.* 26:5389–5397.

12. de Arcuri, B. F., G. F. Vechetti, …, R. D. Morero. 1999. Protein-induced fusion of phospholipid vesicles of heterogeneous sizes. *Biochem. Biophys. Res. Commun.* 262:586–590.

13. Marsh, D. 2007. Lateral pressure profile, spontaneous curvature frustration, and the incorporation and conformation of proteins in membranes. *Biophys. J.* 93:3884–3899.

14. Bayburt, T. H., Y. V. Grinkova, and S. G. Sligar. 2002. Self-assembly of discoidal phospholipid bilayer nanoparticles with membrane scaffold proteins. *Nano Lett.* 2:853–856.

15. Näsvik Öjemyr, L., C. von Ballmoos, …, P. Brzezinski. 2012. Reconstitution of respiratory oxidases in membrane nanodiscs for investigation of proton-coupled electron transfer. *FEBS Lett.* 586:640–645.

16. Bayburt, T. H., and S. G. Sligar. 2010. Membrane protein assembly into Nanodiscs. *FEBS Lett.* 584:1721–1727.

17. Baumann, A., S. Kerruth, …, K. Ataka. 2016. In-situ observation of membrane protein folding during cell-free expression. *PLoS One.* 11:e0151051.

18. Sanchez, K. M., J. E. Gable, …, J. E. Kim. 2008. Effects of tryptophan microenvironment, soluble domain, and vesicle size on the thermodynamics of membrane protein folding: lessons from the transmembrane protein OmpA. *Biochemistry.* 47:12844–12852.

19. MacDonald, R. C., R. I. MacDonald, …, L. R. Hu. 1991. Small-volume extrusion apparatus for preparation of large, unilamellar vesicles. *Biochim. Biophys. Acta.* 1061:297–303.

20. Park, S. H., S. Berkamp, …, S. J. Opella. 2011. Nanodiscs versus macrodiscs for NMR of membrane proteins. *Biochemistry.* 50:8983–8985.

21. Shaw, A. W., M. A. McLean, and S. G. Sligar. 2004. Phospholipid phase transitions in homogeneous nanometer scale bilayer discs. *FEBS Lett.* 556:260–264.

22. Kim, J. E., G. Arjara, …, J. R. Winkler. 2006. Probing folded and unfolded states of outer membrane protein a with steady-state and time-resolved tryptophan fluorescence. *J. Phys. Chem. B.* 110:17656–17662.

23. Keil, B. 1992. Specificity of Proteolysis. Springer Science & Business Media, Berlin, Germany.

24. Krueger, R. J., T. R. Hobbs, …, M. G. Zeece. 1991. Analysis of endoproteinase Arg C action on adrenocorticotrophic hormone by capillary electrophoresis and reversed-phase high-performance liquid chromatography. *J. Chromatogr. A.* 543:451–461.

25. Rodionova, N. A., S. A. Tatulian, …, L. K. Tamm. 1995. Characterization of two membrane-bound forms of OmpA. *Biochemistry.* 34:1921–1929.

26. Ohnishi, S., and K. Kameyama. 2001. Escherichia coli OmpA retains a folded structure in the presence of sodium dodecyl sulfate due to a high kinetic barrier to unfolding. *Biochim. Biophys. Acta.* 1515:159–166.

27. Kang, G., I. Lopez-Pena, …, J. E. Kim. 2013. Probing membrane protein structure and dynamics by fluorescence spectroscopy. *In* Encyclopedia of Analytical Chemistry. R. A. Meyers, ed. John Wiley & Sons, Ltd, pp. 1–21.

28. Shafaat, H. S., K. M. Sanchez, …, J. E. Kim. 2009. Ultraviolet resonance Raman spectroscopy of a β-sheet peptide: a model for membrane protein folding. *J. Raman Spectrosc.* 40:1060–1064.

29. Rawlings, N. D., and G. Salvesen. 2013. Handbook of Proteolytics Enzymes, Third Edition. Elsevier, London.

30. Kleinschmidt, J. H. 2006. Folding kinetics of the outer membrane proteins OmpA and FomA into phospholipid bilayers. *Chem. Phys. Lipids.* 141:30–47.

31. Kleinschmidt, J. H., M. C. Wiener, and L. K. Tamm. 1999. Outer membrane protein A of *E. coli* folds into detergent micelles, but not in the presence of monomeric detergent. *Protein Sci.* 8:2065–2071.

32. Hong, H., and L. K. Tamm. 2004. Elastic coupling of integral membrane protein stability to lipid bilayer forces. *Proc. Natl. Acad. Sci. USA.* 101:4065–4070.

33. Kang, G. P., I. Lopez-Pena, …, J. E. Kim. 2012. Förster resonance energy transfer as a probe of membrane protein folding. *Biochim. Biophys. Acta.* 1818:154–161.

34. Danoff, E. J., and K. G. Fleming. 2015. Membrane defects accelerate outer membrane β-barrel protein folding. *Biochemistry.* 54:97–99.

35. Kleinschmidt, J. H., and L. K. Tamm. 1996. Folding intermediates of a beta-barrel membrane protein. Kinetic evidence for a multi-step membrane insertion mechanism. *Biochemistry.* 35:12993–13000.

36. Schlamadinger, D. E., M. M. Daschbach, …, J. E. Kim. 2011. UV resonance Raman study of cation-π interactions in an indole crown ether. *J. Raman Spectrosc.* 42:633–638.

37. Denisov, I. G., and S. G. Sligar. 2017. Nanodiscs in membrane biochemistry and biophysics. *Chem. Rev.* 117:4669–4713.

38. Rouck, J. E., J. E. Krapf, …, A. Das. 2017. Recent advances in nanodisc technology for membrane protein studies (2012-2017). *FEBS Lett.* 591:2057–2088.

39. McLean, M. A., M. C. Gregory, and S. G. Sligar. 2018. Nanodiscs: a controlled bilayer surface for the study of membrane proteins. *Annu. Rev. Biophys* Published online March 1, 2018. https://doi.org/10.1146/annurev-biophys-070816-033620.

40. Kleinschmidt, J. H. 2015. Folding of β-barrel membrane proteins in lipid bilayers - unassisted and assisted folding and insertion. *Biochim. Biophys. Acta.* 1848:1927–1943.

41. Herrmann, M., B. Danielczak, …, S. Keller. 2015. Modulating bilayer mechanical properties to promote the coupled folding and insertion of an integral membrane protein. *Eur. Biophys. J.* 44:503–512.

42. Anantharamaiah, G. M., J. L. Jones, …, J. P. Segrest. 1985. Studies of synthetic peptide analogs of the amphipathic helix. Structure of complexes with dimyristoyl phosphatidylcholine. *J. Biol. Chem.* 260:10248–10255.

43. Epand, R. M., A. Gawish, …, G. M. Anantharamaiah. 1987. Studies of synthetic peptide analogs of the amphipathic helix. Effect of charge distribution, hydrophobicity, and secondary structure on lipid association and lecithin:cholesterol acyltransferase activation. *J. Biol. Chem.* 262:9389–9396.

44. Miyazaki, M., Y. Tajima, …, M. Nakano. 2010. Static and dynamic characterization of nanodiscs with apolipoprotein A-I and its model peptide. *J. Phys. Chem. B.* 114:12376–12382.

45. Salnikov, E. S., G. M. Anantharamaiah, and B. Bechinger. 2018. Supramolecular organization of apolipoprotein-A-I-derived peptides within disc-like arrangements. *Biophys. J.* 115:467–477.

46. Martinez, D., M. Decossas, …, A. Loquet. 2017. Lipid internal dynamics probed in nanodiscs. *ChemPhysChem.* 18:2651–2657.

47. Kleinschmidt, J. H., and L. K. Tamm. 1999. Time-resolved distance determination by tryptophan fluorescence quenching: probing intermediates in membrane protein folding. *Biochemistry.* 38:4996–5005.

48. Kleinschmidt, J. H., T. den Blaauwen, …, L. K. Tamm. 1999. Outer membrane protein A of *Escherichia coli* inserts and folds into lipid bilayers by a concerted mechanism. *Biochemistry.* 38:5006–5016.

49. Kleinschmidt, J. H. 2003. Membrane protein folding on the example of outer membrane protein A of *Escherichia coli*. *Cell. Mol. Life Sci.* 60:1547–1558.

50. Milan-Garces, E. A., S. Mondal, …, M. Puranik. 2014. Intricate packing in the hydrophobic core of barstar through a CH-pi interaction. *J. Raman Spectrosc.* 45:814–821.

51. Schlamadinger, D. E., J. E. Gable, and J. E. Kim. 2009. Hydrogen bonding and solvent polarity markers in the uv resonance Raman spectrum of tryptophan: application to membrane proteins. *J. Phys. Chem. B.* 113:14769–14778.

52. Chakraborty, H., and B. R. Lentz. 2012. A simple method for correction of circular dichroism spectra obtained from membrane-containing samples. *Biochemistry.* 51:1005–1008.

53. Wallace, B. A., and D. Mao. 1984. Circular dichroism analyses of membrane proteins: an examination of differential light scattering and absorption flattening effects in large membrane vesicles and membrane sheets. *Anal. Biochem.* 142:317–328.

54. Sušac, L., R. Horst, and K. Wüthrich. 2014. Solution-NMR characterization of outer-membrane protein A from *E. coli* in lipid bilayer nanodiscs and detergent micelles. *ChemBioChem.* 15:995–1000.

55. Ishida, H., A. Garcia-Herrero, and H. J. Vogel. 2014. The periplasmic domain of *Escherichia coli* outer membrane protein A can undergo a localized temperature dependent structural transition. *Biochim. Biophys. Acta.* 1838:3014–3024.